

# Ne X X-ray Emission due to Charge Exchange in M82

R. S. Cumbee<sup>1\*</sup>, L. Liu<sup>2</sup>, D. Lyons<sup>1</sup>, D. R. Schultz<sup>3</sup>, P. C. Stancil<sup>1</sup>,  
J. G. Wang<sup>2</sup>, and R. Ali<sup>4</sup>

<sup>1</sup>*Department of Physics and Astronomy and the Center for Simulational Physics, University of Georgia, Athens, GA 30605, USA*

<sup>2</sup>*Institute of Applied Physics and Computational Mathematics, PO Box 8009, Beijing 100088, Peoples Republic of China*

<sup>3</sup>*Department of Physics, University of North Texas, Denton, TX, 76203, USA*

<sup>4</sup>*Department of Physics, The University of Jordan, Amman 11942, Jordan*

## ABSTRACT

Recent X-ray observations of star-forming galaxies such as M82 have shown the  $\text{Ly}\beta/\text{Ly}\alpha$  line ratio of Ne X to be in excess of predictions for thermal electron impact excitation. Here we demonstrate that the observed line ratio may be due to charge exchange and can be used to constrain the ion kinetic energy to be  $\lesssim 500$  eV/u. This is accomplished by computing spectra and line ratios via a range of theoretical methods and comparing these to experiments with He over astrophysically relevant collision energies. The charge exchange emission spectra calculations were performed for  $\text{Ne}^{10+} + \text{H}$  and  $\text{Ne}^{10+} + \text{He}$  using widely applied approaches including the atomic orbital close coupling, classical trajectory Monte Carlo, and multichannel Landau-Zener (MCLZ) methods. A comparison of the results from these methods indicates that for the considered energy range and neutrals (H, He) the so-called “low-energy  $\ell$ -distribution” MCLZ method provides the most likely reliable predictions.

**Key words:** atomic processes - galaxies: individual: M82 - galaxies: starbursts - X-rays: ISM - X-rays: galaxies

## 1 INTRODUCTION

X-ray emission from various solar system environments (Cravens 2000; Lisse et al. 1996; Dennerl 2010; Krasnopolsky et al. 2004) such as comets and planetary atmospheres (Dennerl et al. 2002) has been attributed to de-excitation of highly excited product states following the process of charge exchange (CX). Observations have suggested that CX could be a significant contributor to X-ray emission outside the heliosphere, such as in supernova remnants (Katsuda et al. 2011; Cumbee et al. 2014), starburst galaxies (Liu et al. 2011), and extragalactic cooling flows (Fabian et al. 2011; Lallement 2004).

Within an environment in which both ions and neutral atoms or molecules are present, CX can occur and may dominate the ion emission spectra. During a collision, the ion  $X^{q+}$  captures an electron from a neutral atom creating a highly excited ion  $X^{(q-1)+}(nl\ 2S+1L)$  that then emits one or more photons in a cascade down to the ground state. To accurately model the X-ray emission spectrum and hence better understand neutral and ion density distributions, ion temperatures, and ion charge state distributions in the environments considered, it is essential to include the dominant

collisional processes, including CX, electronic recombination and excitation, and photonic excitation for different relevant ion and neutral interactions.

For example, X-ray line emission has been shown to be prominent in observations of hot plasma environments, and Lallement (2004) and Konami et al. (2011) have suggested that line emission in M82 may partially be due to CX in which a highly ionized plasma collides with cold gas (see also Zhang et al. 2014). Specifically, Konami et al. (2011) suggest that CX emission from Ne X may make a significant contribution to the spectra. A better understanding of the CX emission of Ne X in this environment could help constrain ion and neutral densities in M82 as well as give insight into what other environments CX is prominent.

Here we compare CX X-ray emission due to  $\text{Ne}^{10+}$  collisions with H and He using a number of theoretical methods. In the case of He, X-ray spectra are compared to a previous experiment that used a coincident X-ray - ion charge state and momentum detection approach that allowed determination of the charge exchange product state. Computed Lyman series line ratios are compared to the Ne X  $\text{Ly}\beta/\text{Ly}\alpha$  ratio in the disk of M82 and are found to be consistent with a CX interpretation.

\* rcumbee@physast.uga.edu

## 2 RESULTS AND DISCUSSION

### 2.1 Charge-Exchange Cross Sections

Cross sections for  $\text{Ne}^{10+}$  with H and He for capture to state-resolved  $\text{Ne}^{9+}(n\ell\ ^2L)$  levels have been calculated using the classical trajectory Monte Carlo (CTMC), atomic-orbital close-coupling (AOCC), and multi-channel Landau-Zener (MCLZ) methods. While both collision systems have been studied for many decades (e.g., [Schultz & Krstić 1995](#); [Liu et al. 2014](#)), none of the previous studies have presented a comprehensive set of state-resolved cross sections over a range of energies relevant to astrophysics. The  $\text{Ne}^{10+} + \text{H}$  CX cross sections discussed in this paper are shown in [Figure 1](#) for the dominant capture channel  $n = 6$ . Details of the current MCLZ cross section calculations used here are summarized in [Lyons et al. \(2016\)](#).

The AOCC method for the description of ion-atom collision processes is discussed in detail elsewhere ([Fritsch & Lin 1991](#)). We shall only outline it briefly here. For a one-electron two-center collision system the total electron wave function is expanded over the traveling atomic orbitals centered on each of the two centers (nuclei of the projectile ion and of the target ion). Here, the determination of electronic states centered on the target and on the projectile, is performed by using the variational method with even-tempered trial functions ([Kuang & Lin 1997](#); [Reeves 1963](#)). The total electron wave function  $\Psi$  can be expanded in terms of atomic orbitals, each multiplied by a plane wave electron translational factor (thus giving a traveling atomic orbital  $\Psi$ ). Inserting  $\Psi$  into the time-dependent Schrödinger equation of the collision system, one can get the first-order coupled equations for the amplitudes centered on each of the nuclei. After solving the coupled equations, one obtains the transition amplitudes, whose squared moduli at infinitely large times give the transition probabilities and from them the state-selective CX cross sections that were computed for kinetic energies between 1 and 200 keV/u.

The CTMC method solves an  $n$ -body problem (i.e., consisting of a projectile ion, target nucleus and inactive target electrons, and active target electrons) by solving the classical Hamilton's equations for a large ensemble of projectile-target configurations ("trajectories") to simulate ion-atom collisions ([Abrines & Precival 1966](#); [Olson & Salop 1977](#)).

The trajectories sample initial electronic orbitals prepared to emulate the quantum mechanical electronic momentum distribution. At the end of the trajectory, at some asymptotic distance, relative classical binding energies between particles are computed and used to ascertain whether a reaction (charge exchange, excitation, or ionization) occurred. In the case of charge exchange to produce  $\text{Ne}^{9+}$ , the final  $n\ell$  quantum state is determined based on the binding energy and classical angular momentum of the electron, if bound to the projectile ion, following classical-quantum binning rules ([Becker & MacKellar 1984](#)). Cross sections for H collisions were obtained between 0.1 and 200 keV/u.

### 2.2 X-ray Spectra

In order to predict CX-induced spectra, a low density, steady-state radiative cascade model was applied as described by [Rigazio, Kharchenko, & Dalgarno \(2002\)](#). In this

model, the initial state populations are proportional to the quantum-state-resolved CX cross sections. As the electron cascades down to the lowest energy level, obeying quantum mechanical selection rules, photons are emitted, including X-rays.

When the initial charge  $q$  of the ion  $X^{q+}$  is greater than  $\sim 3$ , the electron will be primarily captured into an excited state that decays to a lower state, such as the ground state, and emits at least one photon. In the case of  $\text{Ne}^{10+} + \text{H}$  that produces the hydrogen-like ion  $\text{Ne}^{9+}$  primarily in the principal quantum level  $n = 6$  (see, for example, [Krasnopolsky et al. 2004](#); [Smith et al. 2014](#)), the electron can be captured to any orbital angular momentum state from  $\ell = 0$  ( $6s$ ) to  $\ell = 5$  ( $6h$ ) with a range of probabilities. In the case that the electron is captured to the  $6p$  state of  $\text{Ne}^{9+}$ , it will primarily decay to the  $1s$  ground state emitting a 1322 eV X-ray photon, the  $\text{Ly}\epsilon$  line. In another case in which the electron is captured to the  $6h$  state, it can only decay by a series of  $\Delta\ell = \Delta n = -1$  Yrast transitions that result in infrared and visible photons. When the electron arrives at the  $2p$  level, it will decay to the ground state emitting the 1020 eV  $\text{Ly}\alpha$  line.  $\text{Ly}\beta$ ,  $\text{Ly}\gamma$ , and  $\text{Ly}\delta$  lines will also be produced from the cascade resulting from capture to other  $6\ell$  states. While  $n = 6$  is the dominant manifold for electron capture with H, there are also significant probabilities for capture to  $n = 7$  and  $n = 5$  followed by cascade and X-ray emission. Therefore, to fully predict the X-ray spectrum of  $\text{Ne}^{9+}$  following CX collisions with H, or similarly with He, requires knowledge of many  $n\ell$ -resolved cross sections.

While the basic CX process has been studied for decades, the existing data are lacking in uniform reliability, in coverage of projectile/target combinations, and in energy ranges relevant to astrophysics. Measurements of state-selective cross sections (i.e., resolved by  $n$  and/or  $\ell$ ) are rare and difficult to perform. The energy resolution is typically poor or the studies are restricted to the measurements of a few final states due to limited detector wavelength ranges. Improvements have been made with experiments to directly measure the X-ray spectrum ([Greenwood et al. 2001](#)), but the measurement is of the total spectrum including the photons from all routes of the cascade. Hence, to directly determine state-selective cross section data, one must turn to theoretical methods. For product ions with more than one electron, or for collisions on He, the status and reliability of calculated cross sections is generally lower than for H. Therefore, there is a need for measured cross sections and for an estimation of them via empirical methods in addition to theoretically predicted results.

In this paper, spectra were obtained for  $\text{Ne}^{10+}$  CX collisions with H and He for a range of kinetic energies. For  $\text{Ne}^{10+} + \text{H}$  CX, cross sections from the AOCC, CTMC, and MCLZ methods are adopted. For the MCLZ method, calculations were performed using the low energy and statistical  $\ell$ -distributions described in equations (15) and (16) of [Janev et al. \(1983\)](#) (see also [Krasnopolsky et al. 2004](#); [Smith et al. 2014](#)). It is necessary to utilize  $\ell$ -distribution functions with MCLZ calculations for product H-like ions (i.e., bare projectiles). Due to degeneracy of a given  $n$ -level in a non-relativistic electronic description, only direct  $n$ -resolved MCLZ computations are possible ([Abramov et al. 1977](#)). Calculations for  $\text{Ne}^{10+} + \text{He}$  CX were performed using only the MCLZ method here, with both the low energy

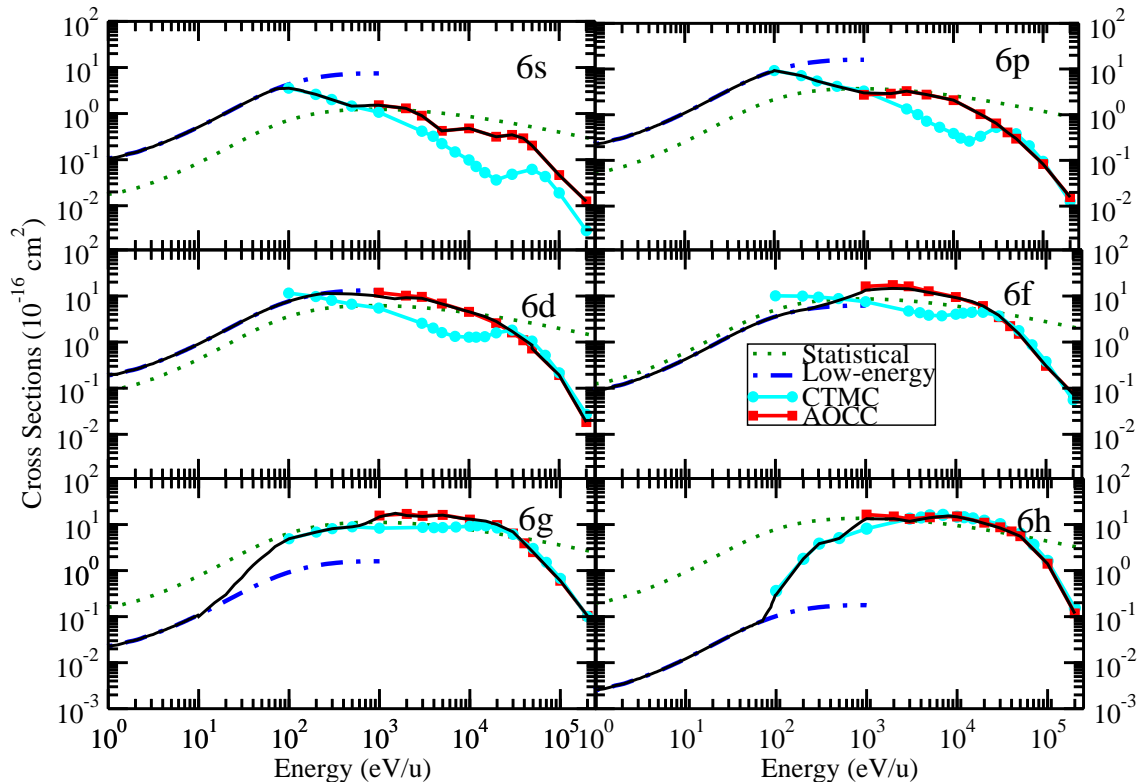


**Figure 1.** New charge exchange cross sections for the collision of  $\text{Ne}^{10+}$  with H as a function of collisional energy for the dominant capture channel of  $n=6$ . The blue (-.-) lines represent the MCLZ low energy distribution, the green dotted (...) lines represent the MCLZ statistical distribution, the cyan lines with filled circles represent the CTMC method, and the red lines with squares represent the AOCC method. The solid black line shows our suggested cross sections.

and statistical  $\ell$ -distributions as with H. Nevertheless, the present (and previously published) AOCC and CTMC data for  $\text{Ne}^{10+} + \text{H}$  CX, applicable primarily at higher impact energies than of astrophysical relevance in nebular environments, are instructive for comparison with MCLZ calculations in order to assess their reasonableness in the range of energies where they have overlapping applicability with CTMC and AOCC. We note below the existence of CTMC data for  $\text{Ne}^{10+} + \text{He}$  CX presented previously in Ali et al. (2010).

Among the theoretical methods for the energy range and ion-atom systems considered here, at lower energies, the MCLZ low energy  $\ell$ -distribution is expected to describe the CX mechanism most accurately. Spectra are shown in Figure 2 for  $\text{Ne}^{10+}$  CX with H and He at collisional energies of 0.1, 0.5, and 1 keV/u using this method.<sup>1</sup> For  $\text{Ne}^{10+}$  CX with H, as the collisional energy increases, the relative intensities of the Ly $\beta$  and higher lines show a slight increase. For

$\text{Ne}^{10+}$  CX with He, the trend is similar for the Ly $\gamma$  line, but reverses for the Ly $\delta$  line. The variation, however, is small. Further, the Ly $\epsilon$  line is practically missing for  $\text{Ne}^{10+} + \text{He}$  as the dominant  $n$  capture channel for CX with He is typically one smaller than for CX with H. Figure 3 shows the similar spectra using the MCLZ statistical distribution. The trends are the same for CX with both H and He, however, for He, the higher Lyman lines have significantly smaller intensities giving a softer total X-ray spectrum. The statistical distribution is likely not valid at this low collision energy. Figures 4-5 show the CTMC, AOCC, and MCLZ low energy and statistical  $\ell$ -distribution spectra for 1-20 keV/u. The most notable difference in comparison to the MCLZ results using the low-energy  $\ell$ -distribution is the decrease in the Ly $\epsilon$  line for all methods.

At higher energies (above  $\sim 1$ -10 keV/u), the statistical  $\ell$ -distribution<sup>2</sup> is expected to be more realistic in describing

<sup>1</sup> All line intensities are normalized such that Ly $\alpha$  has an intensity of 1 and in most cases a Gaussian line-profile with a resolution of 10 eV full-width half-maximum (FWHM) is adopted.

<sup>2</sup> The statistical model assumes that the internal states are populated according to their degeneracy which results from strong rotational mixing at small internuclear separation. Close internuclear distances become accessible for large kinetic energies.

CX emission than the low energy  $\ell$ -distribution. Figure 6 shows the CX emission for  $\text{Ne}^{10+}$  CX with He measured using simultaneous cold-target recoil ion momentum spectroscopy and X-ray spectroscopy as described in Ali et al. (2010) at 4.55 keV/u. The experimental single electron capture (SEC) CX emission is compared to spectra obtained with the CTMC (Ali et al. 2005) and AOCC (Liu et al. 2014) methods at the same energy, and the MCLZ low energy and statistical  $\ell$ -distributions at 4.8 keV/u. Both MCLZ methods provide a better fit to the experimental data than the CTMC or AOCC methods at this energy. The MCLZ statistical  $\ell$ -distribution results in slightly smaller Ly $\beta$  and higher lines, while the MCLZ low-energy  $\ell$ -distribution results in slightly larger Ly $\beta$  and higher lines. At this resolution, the Ly $\beta$  and Ly $\gamma$  lines are not clearly resolved in the theoretical spectra.

In addition to SEC, observed and experimental X-ray emission spectra often contain contributions from multiple electron capture (MEC), including double capture with subsequent autoionization (DCAI) and transfer ionization (TI). Emission from states populated by a combination of these reaction channels may be present in astrophysical spectra. Figure 7 shows a comparison of DCAI to SEC for  $\text{Ne}^{10+}$  CX with He using the CTMC method (Ali et al. 2005). While TI has an insignificant contribution in the present ion-atom systems at low collision energy, DCAI is shown to give a contribution of 21% of the total spectrum for the CTMC method. However, Table 1 in Ali et al. (2005) shows that the experiment suggests a smaller 12% fraction of MEC, which agrees with the MCLZ method from that work. This small fraction of MEC to the total CX emission suggests that ignoring MEC in  $\text{Ne}^{10+}$  CX in an observed spectrum and assuming that SEC is dominant is justifiable when considering He as the CX target, though exceptions for other ions are possible.

### 2.3 Line Ratios

The ratio of the intensity of the Ly $\beta$  and higher lines to the Ly $\alpha$  line vary for different processes and for different collision energies<sup>3</sup>. These ratios can give insight into what processes may be occurring within astrophysical environments, including, but not limited to, extracting the collisional energies and ion abundance ratios. Figures 8-9 show the ratios of Ly $\beta$ /Ly $\alpha$  calculated over different collisional energies using the four different methods described in §2.1. Because the astrophysical environments of present interest contain both neutral H and He, line ratios for the collisions of  $\text{Ne}^{10+}$ +H (Fig. 8), He (Fig. 9), and for the assumed fraction of 90% H and 10% He (Fig. 9 for the MCLZ calculations) are shown.

For  $\text{Ne}^{10+}$  CX with H, the MCLZ statistical  $\ell$ -distribution and AOCC line ratios are almost equal at 1 keV/u, and are relatively consistent between 1 and 10 keV/u. The CTMC method is very similar to the AOCC results for the range of 10-50 keV/u considered. The MCLZ low energy  $\ell$ -distribution method, however, gives a line ratio

<sup>3</sup> Cross sections and line ratios are available upon request, but will be made available through the automated package Kronos (Mullen et al. 2016), which contains a database of our preliminary H-like and He-like MCLZ CX cross sections.

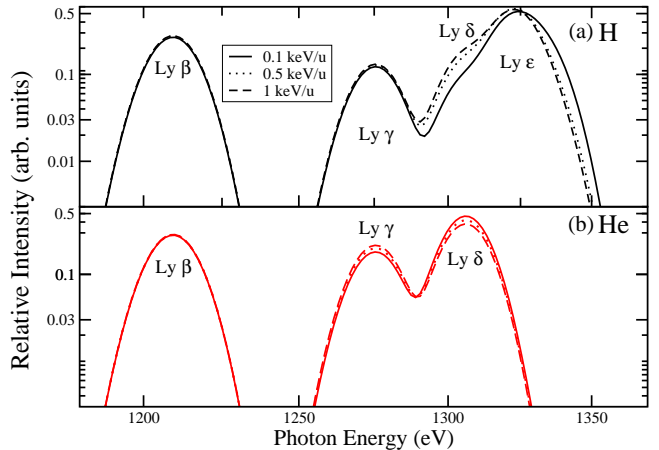


**Figure 2.** X-ray spectra using the MCLZ cross sections with the low energy  $\ell$ -distribution are shown for the collisions of  $\text{Ne}^{10+}$  with H (top panel) and He (bottom panel) at collisional energies of 0.1, 0.5 and 1 keV/u. Lines are normalized to Ly $\alpha$  (not shown) at 1020 eV with a resolution of 10 eV FWHM.

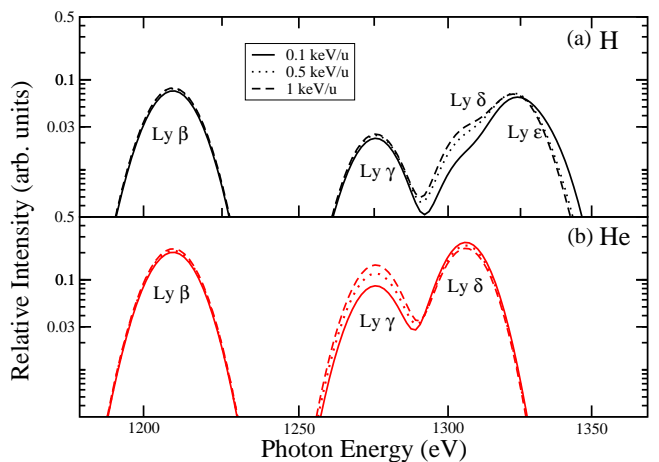


**Figure 3.** X-ray spectra using the MCLZ cross sections with the statistical  $\ell$ -distribution are shown for the collisions of  $\text{Ne}^{10+}$  with H (top panel) and He (bottom panel) at collisional energies of 0.1, 0.5 and 1 keV/u.

over an order of magnitude larger than all other methods for the entire energy range. The low energy  $\ell$ -distribution is expected to be more relevant at lower energies than the AOCC or CTMC methods, as suggested in Figure 6. However, extending the CTMC method to lower energies, it appears to approach the MCLZ low energy  $\ell$ -distribution for  $E \lesssim 0.1$  keV/u. It can then be postulated that the transition from statistical to low-energy  $\ell$ -distributions occurs between  $\sim 0.1$

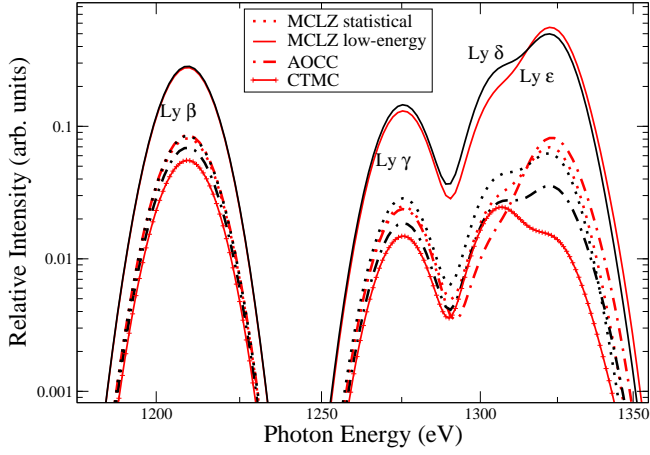


**Figure 4.**  $\text{Ne}^{10+} + \text{H}$  X-ray spectra calculated using the AOCC and CTMC cross sections are compared to the MCLZ method at collisional energies of 1 keV/u (black lines) and 5 keV/u (red lines).

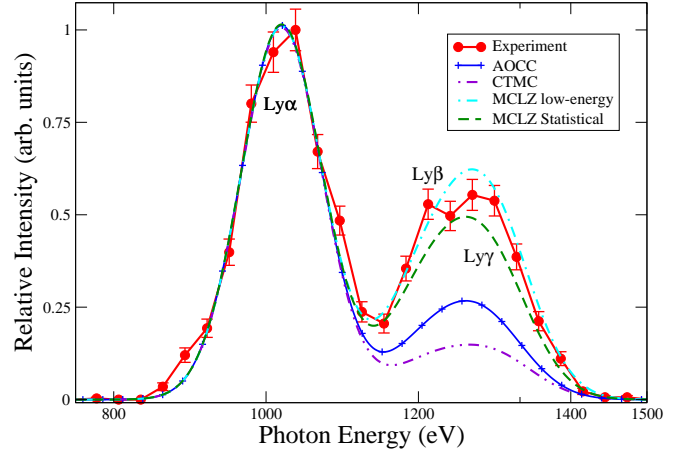


**Figure 6.** Experimental single electron capture (SEC) data for  $\text{Ne}^{10+}$  CX with He at  $\sim 4.5$  keV/u is compared to CTMC, AOCC (Liu et al. 2014), and MCLZ low-energy and statistical distributions for SEC. A resolution of 75 eV FWHM is used for the theoretical methods compared to a resolution of 68 eV for the experimental data (Ali et al. 2010). Note that the experimental spectra includes no multi-electron capture events.

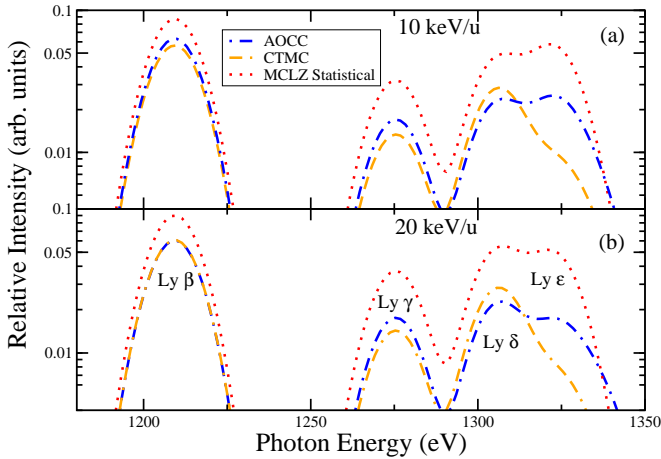


**Figure 5.** The CTMC method is compared to the AOCC and MCLZ statistical  $\ell$ -distribution methods for the collision of  $\text{Ne}^{10+}$  with H at an energy of 10 keV/u (top panel) and 20 keV/u (bottom panel).

and 1 keV/u making the MCLZ low energy  $\ell$ -distribution relevant at energies less than  $\sim 0.5$  keV/u.

For  $\text{Ne}^{10+}$  CX with helium, MCLZ cross sections have been computed in the present work down to low energy ( $\sim 100$  eV/u) and CTMC results at one impact energy (4.5 keV/u, Ali et al. 2010) are available from previous work, though they could easily be extended to higher and lower energies. These results are shown in Figure 9 along with

the experimental (Ali et al. 2010) and the AOCC (Liu et al. 2014) results at 4.55 keV/u.

### 3 APPLICATION TO M82

In Figures 8-9, the  $\text{Ly}\beta$  to  $\text{Ly}\alpha$  ratios for  $\text{Ne}^{10+}$  CX with H and He are overlaid with line ratio observations (vertical lines) for M82 from *Suzaku* described by Konami et al. (2011). The observations give the  $\text{Ne}^{9+}$   $\text{Ly}\beta$  to  $\text{Ly}\alpha$  ratio for four different regions in M82; the Disk, Wind-1, Wind-2, and Wind-3. In their Figure 8, Konami et al. (2011) showed that the line ratios for the three Wind regions can be reproduced by a collisional ionization equilibrium (CIE) model, but the Disk region cannot. The  $\text{Ly}\beta$  to  $\text{Ly}\alpha$  ratio from the CIE model is significantly smaller at  $\sim 0.1$  than the observed Disk line ratio ( $\sim 0.25$ ), indicating that the line ratio in the Disk might be primarily due to CX. Assuming that CX has a significant contribution to the spectrum of M82, the collisional energies at which the  $\text{Ly}\beta$  to  $\text{Ly}\alpha$  line ratios cross the observed line ratio from Konami et al. (2011) gives a constraint on the ion kinetic energy in M82.<sup>4</sup>

Figures 8 and 9 show that the MCLZ low energy  $\ell$ -distribution line ratios agree with the Disk region observation by Konami et al. (2011) for H and He over a wide range

<sup>4</sup> The Ne IX  $K\beta$  line at 1074 eV may partially overlap the observed Ne X  $\text{Ly}\alpha$  line contaminating the line ratio. The  $K\beta$  is expected, however, to account for less than  $\sim 5\%$  of the Ne IX emission and the removal of its contribution would only enhance the  $\text{Ly}\beta/\text{Ly}\alpha$  ratio.

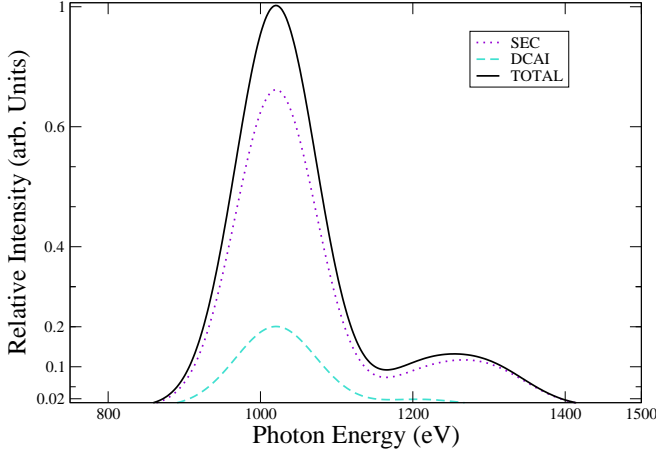


**Figure 7.**  $\text{Ne}^{10+} + \text{He}$  SEC is compared to DCAI and the summed total for the CTMC method with a 75 eV FWHM resolution. SEC dominates the total with 79% while DCAI contributes 21% of the total.

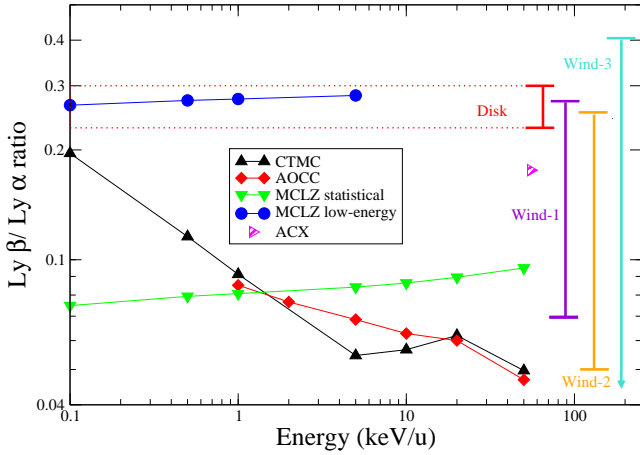


**Figure 8.** Line ratios ( $\text{Ly}\beta/\text{Ly}\alpha$ ) for the three methods shown in Figures 3-5 as a function of collisional energy for charge exchange of  $\text{Ne}^{10+}$  with H. The vertical lines represent the Disk, Wind-1, Wind-2, and Wind-3 regions of M82 as described by Konami et al. (2011). The results from the ACX model (Zhang et al. 2014) are also shown. Note that the results from Konami et al. (2011) and Zhang et al. (2014) have no ion kinetic energy dependence and their placement on the right side of the plot is arbitrary.

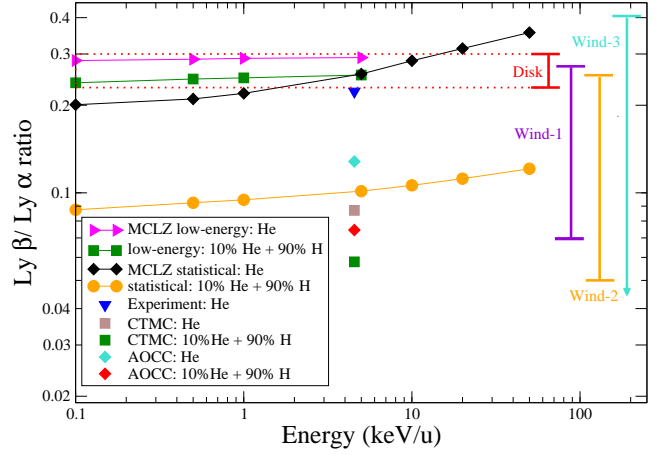


**Figure 9.** Same as Figure 8 but for the collision of  $\text{Ne}^{10+}$  with He. Also shown is the addition  $\text{Ne}^{10+}$  with 90% H and 10% He, which is the assumed ratio of the He to H charge exchange contributions. CTMC, AOCC, and experimental  $\text{Ne}^{10+} + \text{He}$  data at 4.55 keV/u (see Figure 6) are also compared.

of ion energies (0.1 to 5 keV/u), while the CTMC line ratio for H approaches the observational result near 0.1 keV/u. The MCLZ low energy  $\ell$ -distribution is over an order of magnitude higher than all other methods for the entire energy range in Figure 8, making it fall within the range of the Disk line ratio for M82. As postulated above, the transition from statistical to a low-energy  $\ell$ -distribution occurs between 0.1 and 1 keV/u, because the low energy  $\ell$ -distribution  $\text{Ly}\beta$  to  $\text{Ly}\alpha$  ratio curve lies within the Disk region uncertainty, we can postulate that the ion kinetic energy in the disk is likely  $\lesssim 0.5$  keV/u (300 km/s).

In the more unlikely case that all of the atomic H in the Disk region has been ionized leaving only neutral He, Figure 9 shows that again the  $\text{Ly}\beta/\text{Ly}\alpha$  ratio predicted by the MCLZ cross sections with the low-energy  $\ell$ -distribution gives best agreement. The MCLZ statistical distribution for He predicts line ratios in agreement with the *Suzaku* observation for ion velocities of  $\sim 950$ -2000 km/s (1-10 keV/u). Likewise, the measurements of Ali et al. (2010) performed at 930 km/s are also consistent with the Disk observation, but these high ion velocities likely cannot be produced in starburst outflows. The CTMC and AOCC He results underestimate the observation by a factor of  $\sim 3$  at the energy for which data are available, namely, about 4.5 keV/u, which is considerably larger than the estimated 0.5 keV/u identified above as the likely maximum ion energy that is relevant to CX in the Disk region.

Considering CX from both H and He, but with abundance fractions of 90% and 10%, respectively, again the MCLZ low-energy distribution result agrees best with the observations in the Disk region. For all other methods, He target contributions increase the predicted  $\text{Ly}\beta/\text{Ly}\alpha$  ratio, but only to  $\sim 0.1$  at 4.55 keV/u (930 km/s).

Using *XMM-Newton* observations with its Reflection

Grating Spectrometer (RGS), Zhang et al. (2014) modeled the X-ray spectrum of M82 assuming a two component model consisting of hot single-temperature thermal plasma emission (electron-impact excitation) and CX emission. They found that the Ne X Ly $\alpha$  line intensity can be reproduced if 19% of the emission is due to CX. However, the RGS spectrum covers the entire disk and outflow of M82 (i.e., Disk, Wind-1, Wind-2, and Wind-3 regions of Konami et al. 2011). This is consistent with the suggestion of Konami et al. that the Wind components can be modeled with thermal emission, while the Disk is dominated by CX emission, the latter confirmed here. Further, the CX contribution in Zhang et al. (2014) was obtained with the AtomDB Charge eXchange (ACX) model (Smith et al. 2012) that adopted the so-called separable  $\ell$ -distribution. The low-energy distribution peaks at  $\ell = 1$ , while the separable distribution peaks at  $\ell = 2$  for Ne<sup>10+</sup> that results in the ACX Ly $\beta$ /Ly $\alpha$  ratio of 0.176, shown in Figure 8. This line ratio is somewhat smaller than the observed Disk ratio of  $\sim 0.28$  with *Suzaku*, but consistent with total line ratio of 0.182 Zhang et al. (2014) measured with the RGS. However, one must remember the *XMM-Newton*/RGS measurement includes all regions of the Disk and outflow.

To reproduce the observed Disk Ly $\beta$ /Ly $\alpha$  ratio assuming only CX emission, our modeling suggests that the relative ion velocity is  $\lesssim 300$  km/s, independent of whether a 10% He component is included. While superwind models of the M82 outflow typically adopt velocities greater than 1000 km/s, Zhang et al. (2014) suggest that a reasonable approximation is closer to  $\sim 500$  km/s. Finally, a further test of the contribution of CX to the X-ray emission could be made by modeling the Ly $\delta$  and Ly $\epsilon$  emission at 1308 and 1325 eV, respectively. Figure 2 suggests that both line intensities (for H) are larger than or comparable to that of Ly $\beta$ . The Ly $\epsilon$  to Ly $\delta$  ratio could be used to constrain the neutral He to H fraction given the negligible Ly $\epsilon$  emission for Ne<sup>10+</sup> + He collisions. In fact, there is some hint of this feature in the CX modeling of Zhang et al. (2014), though blending of the Mg XI K $\alpha$  forbidden line may contaminate the Ne lines. Higher resolution spectra, such as with *Hitomi* will better resolve the emission lines and allow for better constraints on the contribution of Ne X CX. A more thorough model, using for example, XSPEC (Arnaud et al 1996), should be performed including H and He-like C, N, O, Ne, Mg, and Si and Fe XVII ions colliding with H and He targets, similar to the approach of Zhang et al. (2014), but with reliable CX data. Such a comprehensive approach would help in determining the contribution of various mechanisms including, collisional excitation (CIE), radiative recombination, CX, or other processes such as active galactic nuclei (AGN) activity.

#### 4 CONCLUSIONS

As shown here via our comparison of results of various conventional theoretical approaches, the MCLZ low-energy  $\ell$ -distribution is likely the better method for producing Ne<sup>10+</sup> CX line ratios with H and He below 5 keV/u. The statistical distribution may be used above 1 keV/u, but the AOCC method is preferred. As the AOCC and CTMC methods have agreement between 10 and 50 keV/u, either method would work, but as the Ly $\epsilon$  lines (due to H) are similar for

the MCLZ statistical and AOCC methods for this energy, the AOCC approach is likely more accurate.

The current charge exchange modeling of the Ne X X-ray emission for the Disk of the starburst galaxy M82 suggests that CX may account for the observed Ly $\beta$ /Ly $\alpha$  ratio, a ratio that is not consistent with thermal emission due to electron-impact excitation. Further, the emission may include contributions from CX with neutral H and He suggesting a relative ion velocity of  $\lesssim 300$  km/s. While cross sections obtained with the multichannel Landau-Zener method using the so-called low-energy  $\ell$ -distribution model predicts X-ray line ratios consistent with the observations, calculations using the theoretical method known as the molecular-orbital close-coupling approach, recognized to be among the most complete treatments of ion-atom collisions at low-impact energies, but with significantly greater computational effort and complexity, should be made to confirm these results.

#### ACKNOWLEDGMENTS

The work of RSC, DL, DRS, and PCS was partially supported by NASA grants NNX09AC46G and NNX13AF31G. RSC acknowledges support from NSF East Asian and Pacific Summer Institute and the Chinese Academy of Sciences and thanks those at the IAPCM for hosting her at the beginning of this project as well as Adam Foster, Randall Smith, and Shuinai Zhang for helpful discussions. We thank the referee for providing useful comments which improved the manuscript.

#### REFERENCES

- Abramov, V. A., Baryshnikov, F. F., & Lisitsa, V. S. 1977, *Sov. Phys. JETP*, 47, 469
- Abrines, R. & Precival, I. C. 1966, *Proc. Phys. Soc.*, 88, 861
- Ali, R., Neill, P. A., Beiersdorfer, P., Harris, C. L., Rakovič, M. J., Wang, J. G., C. Schultz, D. R., & Stancil, P. C. 2005, *ApJL*, 629, L125
- Ali, R., Neill, P. A., Beiersdorfer, P., Harris, C. L., Schultz, D. R., & Stancil, P. C. 2010 *ApJL*, 716, L95
- Arnaud, K.A. 1996, *Astronomical Data Analysis Software & Systems V*, eds. Jacoby G. & Barnes J., p. 17, *ASP Conf. Series* vol. 101
- Baird, S.R. 1981, *ApJ*, 245, 208
- Beckar, R. L. & MacKellar, A. D. 1984, *J. Phys. B*, 17, 3923
- Cravens, T. E. 2000, *ApJ*, 532, L153
- Cumbee, R. S., Henley, D. B., Stancil, P. C., Shelton, R. L., Nolte, J. L., Wu, Y., and Schultz, D. R. 2014, *ApJ*, 787, L31
- Dennerl, K. 2010, *SSR*, 157, 57
- Dennerl, K., Burwitz, V., Englhauser, J., Lisse, C., & Wolk, S. 2002, *A&A*, 386, 319
- Fabian, A. C., Sanders, J. S., Williams, R. J. R. Lazarian, A., Ferland, G. J., & Johnstone, R. M. 2011, *MNRAS*, 417, 172
- Fritsch, W. & Lin, C. D. 1991, *Phys. Rep.*, 202, 1
- Greenwood, J. B. Williams, I. D., Smith, S. J., & Chutjian, A. 2001, *Phys. Rev. A*, 63, 062707
- Janev, R. K., Belic, D. S., & Brandsden, B. H. 1983, *Phys. Rev. A*, 1293, 28
- Katsuda, S., Tsunemi, H., Mori, K., Uchida, H., Kosugi, H., Kimura, M., Nakajima, H., Takakura, S., Petre R., Hewitt, J. W., & Yamaguchi, H. 2011, *ApJ*, 730, 24
- Konami, S., Tsuru, T. G., Gandhi, P., & Tamagawa, T. 2011, *PASJ*, 63, S913

- Krasnopolsky, V., Greenwood, J., & Stancil, P. C. 2004, SSR, 113, 271
- Kuang, J. & Lin, C. D. 1997, J. Phys. B, 30, 101
- Lallement, R. 2004, A&A, 422, 391
- Lisse, C. M. *et al.* 1996, Science, 274, 205
- Liu, J., Mao, S., & Wang, Q. D. 2011, MNRAS., 415, L64
- Liu, L., Wang, J. G., & Janev, R. K. 2014, Phys. Rev. A, 89, 012710
- Lyons, D., Cumbee, R. S., & Stancil, P. C. 2016, to be submitted
- Mullen, P. D., Cumbee, R. S., Lyons, D. & Stancil, P. C. 2016, ApJS, In Press
- Olson, R.E. & Salop, A. 1977, Phys. Rev. A, 16, 531
- Reeves, C. M. 1963, J. Chem. Phys. 39, 1
- Rigazio, M., Kharchenko, V., & Dalgarno, A. 2002, Phys. Rev. A, 66, 064701
- Schultz, D. R. & Krstić, P.S. 1995, Atomic and Plasma-Material Interaction Data for Fusion, 6, 173
- Smith, R. K., Foster, A. R., & Brickhouse, N. S. 2012, AN, 333, 301
- Smith, R. K., Foster, A. R., Edgar, R. J., & Brickhouse, N. S. 2014, ApJ, 787, 77
- Zhang, S., Wang, Q. D., Ji, L., Smith, R. K., Foster, A. R., & Zhou, X. 2014, ApJ, 794, 61

# New features in the *Monthly Notices* L<sup>A</sup>T<sub>E</sub>X 2<sub>ε</sub> class file

2001 February 06

The MNRAS L<sup>A</sup>T<sub>E</sub>X 2<sub>ε</sub> class file is implemented by placing the command `\documentclass[options]{mn2e}` at the start of the document.

The various `option` commands listed in the *Monthly Notices* L<sup>A</sup>T<sub>E</sub>X style guide for authors can still be used. The following additional options exist.

(i) `useAMS` – this enables the production of upright Greek characters  $\pi$ ,  $\mu$  and  $\partial$  (`\upi`, `\umu` and `\upartial`) and slanted  $\leq$  and  $\geq$  (`\leq` and `\geq`). Characters  $\pi$ ,  $\mu$  and  $\partial$  appear upright only on systems that have the Euler roman fonts (`eurmxx`); characters  $\leq$  and  $\geq$  appear slanted only on systems that have the AMS series A fonts (`msamxx`). On systems that do not have these fonts, the standard forms of the characters appear in the printout; however, they should be correct in the final typeset paper if the correct L<sup>A</sup>T<sub>E</sub>X commands have been used.

(ii) `usedcolumn` – this uses the package file `dcolumn.sty` to define two new types of column alignment for use in tables. If the `usedcolumn` option has been specified then, within a table, `d{x}` can be used to produce a ‘flush right’ decimal-aligned column with  $x$  decimal places and `.` can be used to provide a decimal-aligned column centred on the decimal point (the number of decimal places does not need to be specified for this column type). Note that the standard L<sup>A</sup>T<sub>E</sub>X ‘tools’ packages `dcolumn.sty` and `array.sty` are required in order to use the `usedcolumn` option.

(iii) `usenatbib` – this uses Patrick Daly’s `natbib.sty` package for cross-referencing. If the `usenatbib` option is specified, citations in the text should be in one of the following forms (or one of the additional forms documented within `natbib.sty` itself).

- `\citet{key}` produces text citations, e.g. Jones et al. (1990),
- `\citep{key}` produces citations in parentheses, e.g. (Jones et al. 1990),
- `\citealt{key}` produces citations with no parentheses, e.g. Jones et al. 1990.

For three-author papers, a full author list can be forced by putting a `*` just before the `{`. To add notes within the citation, use the form `\citep[pre-reference-text][post-reference-text]{key}` (note that either of `pre-reference-text` and `post-reference-text` can be blank).

Items in the reference list must be of the form

```
\bibitem[\protect\citeauthor{author_names}{year}]{key} Text of reference ...
```

for one-, two- and multi-author papers, or

```
\bibitem[\protect\citeauthor{three_author_names}{first_author_etal}{year}]{key} Text of reference ...
```

for three-author papers.

Note that Patrick Daly’s package `natbib.sty` is required in order to use the `usenatbib` option.

We recommend that authors use `natbib.sty` as their standard cross-referencing package, because of the flexibility in citation style that it provides.

(iv) `usegraphicx` – this loads the graphics package `graphicx.sty`, which authors can use to include figures in their papers. Note that the standard L<sup>A</sup>T<sub>E</sub>X graphics package `graphicx.sty` is required in order to use the `usegraphicx` option.

Other style files, or packages providing features such as graphics support, can be used in conjunction with `mn.cls`. To do this, the command `\usepackage{package_name}` is used.

An additional feature of the class file is that footnote symbols are now in the correct journal style (symbols for title page footnotes, superscript arabic numbers for text footnotes).

A BibTeX style file, `mn2e.bst`, is now available for authors who wish to use BiBTeX. It is recommended that this should be used in conjunction with `natbib.sty`.

For general instructions on preparing *Monthly Notices* papers in L<sup>A</sup>T<sub>E</sub>X, please refer to the MNRAS L<sup>A</sup>T<sub>E</sub>X style guide for authors, available on the CTAN sites in subdirectory `/tex-archive/macros/latex209/mnras`.